*Journal of Statistical Physics, Vol. 100, Nos. 1/2, 2000*

# Applications of Integral Equation Calculations to High-Temperature Solvation Phenomena

**A. A. Chialvo,[1, 2, *] P. G. Kusalik,[5] Yu. V. Kalyuzhnyi,[6] and P. T. Cummings[2, 3, 4, 7]**

*Received August 16, 1999*

The solvation of infinitely dilute solutes in supercritical solvents is illustrated by integral equation calculations, according to a recently proposed molecular-based formalism that characterizes the solvent environment around individual species and connects it to the resulting macroscopic solvation behavior. The formalism is applied to the analysis of the solubility enhancement of nonelectrolyte species, the solvent effect in kinetic rate constants, and the solvation of ionic species. Finally, some relevant theoretical implications are discussed regarding the modeling of high-temperature solutions.

**KEY WORDS:** High-temperature solvation thermodynamic; molecular asymmetry; supercritical fluids; solvation formalism; aqueous electrolyte solutions; solvation effects on kinetic rate constants; solute-induced effects; compressibility-driven phenomena.

---

This manuscript has been authored by a contractor of the U.S. Government under contract No. DE-AC05-96OR22464. Accordingly, the U.S. Government retains a nonexclusive, royalty-free license to publish or reproduce the published form of this contribution, or allow others to do so, for U.S. Government purposes.

[1] Chemical and Analytical Sciences Division, Oak Ridge National Laboratory, Oak Ridge, Tennessee 37831-6110.

[2] Department of Chemical Engineering, University of Tennessee, Knoxville, Tennessee 37996-2200.

[3] Department of Chemistry, University of Tennessee, Knoxville, Tennessee 37996-2200.

[4] Department of Computer Science, University of Tennessee, Knoxville, Tennessee 37996-2000.

[5] Department of Chemistry, Dalhousie University, Halifax, Nova Scotia, B3H 4J3, Canada.

[6] Institute for Condensed Matter Physics, 290011 Lviv, Ukraine.

[7] Chemical Technology Division, Oak Ridge National Laboratory, Oak Ridge, Tennessee 37831-6268.

* To whom correspondence should be addressed.



0022-4715/00/0700-0167$18.00/0 © 2000 Plenum Publishing Corporation

## 1. INTRODUCTION

The molecular-based understanding of the solvation process taking place when a species is introduced in a pure solvent at near- and supercritical conditions has been the goal of many researchers in the physical chemistry community.[1, 2] In particular, chemical engineers have been most interested in the potential uses of supercritical fluids in a variety of industrial processes, ranging from extraction of value-added components in the food industry[3, 4] to their use as media to conduct chemical reactions,[5, 6] according to their ability to tailor the solvation behavior of species in solution. In addition, nature provides numerous examples of hydrothermal processes that take place in high-temperature aqueous media, which involve the simultaneous solvation of gases, non-polar compounds, and salts.

A common, and frequently overlooked, feature in all these systems is the simultaneous occurrence of microscopic phenomena involving two rather different length scales.[7] That is, the introduction of a foreign species in an otherwise pure solvent, induces a finite (and local) density perturbation (the solvation structure), whose effect propagates over a distance across the solvent given by the prevalent correlation length. This propagation is compressibility driven, and therefore, all mechanical properties of the infinitely dilute species in solutions will scale as the pure solvent compressibility.[8] In fact, as the infinitely dilute systems approaches the solvent's critical condition, the solvation contributions may be obscured by the diverging critical quantities so that it is imperative for us to be able separate the two contributions.

While the coexistence of both short- (solvation) and long-ranged (compressibility driven) effects makes supercritical solutions challenging to model, this feature suggests a natural way to characterize their thermodynamic properties in terms of the two distinct length scales. Moreover, this precise characterization highlights the explicit contributions of molecular solute-solvent asymmetry to the solvation phenomenon. Beyond a curiosity, and the fact that supercritical fluids are widely used in chemical engineering, the occurence of the compressibility-driven phenomena stresses the need for new tools to isolate the unwanted and rather annoying divergent quantities.

Most theoretical studies on supercritical fluids in general, and supercritical solvation in particular, have focussed on the underlying connection between the species partial molar properties and the system microstructure.[9–11] While these studies were motivated by the urgency for rigorous methods based on statistical mechanics, progress was only made after we recognized and performed the unambiguous split between solvation and compressibility-driven contributions to the system properties. This split was

achieved according to the length scales involved and independently of any arbitrary choice for the size (radius) of the solvation shell.[7, 12]

In this report we succinctly review our solvation formalism for infinitely dilute supercritical solutions by exhibiting some statistical mechanical expressions relevant to supercritical solvation and the connection to their thermodynamic counterparts. Then we illustrate the formalism using integral equation calculations for supercritical systems composed of either Lennard-Jones, Yukawa, or hard spheres plus multipoles and polarizabilities. These systems will be used to analyze the behavior of some relevant macroscopic solvation properties associated with solubility enhancement and solvent effects on kinetics (Lennard-Jones), gas solubility (Yukawa), and ionic solvation (hard-spheres plus multipoles and polarizabilities).

This report is organized as follows. In Section 2 we introduce the main ideas behind the solvation formalism. Subsequently, in Subsections 2.1 to 2.4, we discuss some specific features associated with the solubility enhancement of solutes, the solubility of gases, the solvent effects on kinetic rate constants, and the solvation of ions, respectively, in supercritical solvents. In Section 3, Subsections 3.1 to 3.4, we illustrate the solvation phenomena discribed in the previous sections with integral equations calculations. Finally, in Section 4, we provide some relevant comments regarding the solvation formalism and the macroscopic modeling of high-temperature solutions.

## 2. SOLUTE-INDUCED EFFECTS AND SUPERCRITICAL SOLVATION

The solvation formalism[7, 12, 13] hinges upon the discrimination between the local solvent-density perturbation due to the presence of the solute (as opposed to a solvent molecule), and the concomitant compressibility-driven propagation of this perturbation. From a pictorial viewpoint the solvation of a solute molecule $U$ in a pure solvent $V$ at constant state conditions (constant temperature $T$ and either constant pressure $P$ or solvent density $\rho$) can be described by a *thought experiment* on a system (pure solvent) in which one solvent molecule $V$ is distinguishable by its *solute* label $U$. As such, this system constitutes an *ideal solution* in the sense of the Lewis-Randal rule.[14, 15] Consequently, the solvation process proceeds by the mutation of the distinguishable solvent molecule $U$ into the actual solute molecule $U$ (e.g., through a Kirkwood coupling-parameter charging) to form the desired infinitely dilute *non-ideal solution*. This process in which the original *solute* species $U$ in the *ideal solution*—where solute-solvent $UV$-interaction are identical to solute-solute $UU$- and

solvent-solvent $VV$-interactions—is converted into the actual solute $U$ in the non-ideal solution, is driven by the difference of free energy $(\mu_U^{r\infty}(T, P) - \mu_V^{ro}(T, P))$, where $\mu$ is the chemical potential, the supercript $r$ denotes a residual quantity for a pure $(o)$ or an infinitely dilute $(\infty)$ species at the indicated state conditions, respectively. Note that for electrolyte solutions the solvation process involves $v$ *solute* species in the *ideal solution* and the difference of free energy becomes $(\mu_U^{r\infty}(T, P) - v\mu_V^{ro}(T, P))$, where $v = v_+ + v_-$, with $v_+$ and $v_-$ being the stoichiometric coefficients of the salt (see Section 2.4).

In brief, this formalism connects the microscopic changes of the solvent structure around the mutating species with the macroscopic (thermodynamic) properties which best characterize the solvation process at high-temperature, while segregating the solvation from the compressibility phenomena. As we discussed elsewhere[16] this connection can be achieved in essentially four equivalent ways, by interpreting the driving force of the solvation process from either a microscopic or a macroscopic perspective. For convenience of notation throughout the paper, we first take the neutral ionic solute as our hypothetical "molecular" entity $U$ in order to derive the solvation quantities. Thus, when dealing with non-electrolyte solutions we should replace $v = 1$ in all derived expressions.

We start with the exact thermodynamic expression,[13]

$$\mu_U^{r\infty}(T, P) - v\mu_V^{ro}(T, P) = vkT \ln(\hat{\phi}_U^{\infty}/\hat{\phi}_V^{o}) = \int_0^{\rho(P)} (\bar{v}_U^{\infty} - v\bar{v}_V^{o}) \frac{d\rho}{\kappa\rho} \qquad (1)$$

where $k$ is the Boltzmann constant, $\bar{v}_V^o = \rho^{-1}$ is the partial molar volume of the pure solvent, $\hat{\phi}_i$ is the partial molar fugacity coefficient of species $i$, and $\kappa$ is the solvent isothermal compressibility. Now, we can introduce the rate of change of pressure (at constant temperature and solvent density) caused by the structural perturbation of the solvent around the solute, i.e., $(\partial P/\partial x_U)_{T,\rho}^{\infty}$ as follows,[13]

$$\mu_U^{r\infty}(T, P) - v\mu_V^{ro}(T, P) = \int_0^{\rho(P)} \left(\frac{\partial P}{\partial x_U}\right)_{T,\rho}^{\infty} \frac{d\rho}{\rho^2} \qquad (2)$$

Equation (2) highlights the finiteness of its integrand at any state condition, and allows us to make contact with the microstructure of the system,[12] i.e., (see Appendix B of Chialvo *et al.*[13]),

$$\left(\frac{\partial P}{\partial x_U}\right)_{T,\rho}^{\infty} = v\rho kT(C_{VV}^{o} - C_{UV}^{\infty}) \qquad (3)$$

where $C^{o}_{VV}$ and $C^{\infty}_{UV}$ are the direct correlation function integrals (DCFI) for the solvent-solvent and solute-solvent interactions (i.e., $c_{ij}(\mathbf{k})$ is the three-dimensional Fourier transform of the direct correlation function $c_{ij}(r)$, then $C_{ij} \equiv \rho \hat{c}_{ij}(\mathbf{k}=\mathbf{0})$ are descriptors of the solution microstructure[17, 18]).

Because the experimental microscopic information is typically in the form of correlation functions, a convenient way of looking at the solvation driving-force is in terms of integrals over those functions such as the excess particle-number,[12]

$$N^{\infty}_{U,\,ex} = 4\pi\rho \int_0^{\infty} [\, g^{\infty}_{UV}(r) - g^{o}_{VV}(r) \,]\, r^2\, dr \tag{4}$$

i.e., the number of solvent molecules around the solute in excess of that around any solvent molecule (the Lewis-Randall ideal solution). Because $N^{\infty}_{U,\,ex} = -\kappa(\partial P/\partial x_U)^{\infty}_{T,\,\rho}$,[12] we can also show that its solvation contribution becomes $N^{\infty}_{U,\,ex}(SR) = (\kappa^{IG}/\kappa)\, N^{\infty}_{U,\,ex}$,[16] and consequently,

$$\left(\frac{\partial P}{\partial x_U}\right)^{\infty}_{T,\,\rho} = -\frac{N^{\infty}_{U,\,ex}(SR)}{\kappa^{IG}} \tag{5}$$

where $\kappa^{IG} = (\rho kT)^{-1}$ is the isothermal compressibility of the ideal gas at the same state conditions as the solvent, and $SR$ denotes short-ranged (associated with the local solvent density-perturbation) contribution to the corresponding diverging $N^{\infty}_{U,\,ex}$. Equation (5) emphasizes the connection between the pressure change associated with the perturbation of the solvent structure around the solute and the corresponding *effective* change in the number of solvent molecules. The notation $SR$ can equally well be interpreted to mean solvation-related to distinguish it from the long-ranged, or compressibility-related quantities.

The ourstanding feature of $N^{\infty}_{U,\,ex}(SR)$ is its independence from any choice for the radius of the solvation shell, therefore, it can be thought as being an *effective* solvation number (see Chialvo *et al.*[13]). However, it should not be confused with the conventional definition of hydration/solvation numbers based on the structural information for the first hydration shell.

Analogously, the pressure derivative $(\partial P/\partial x_U)^{\infty}_{T,\,\rho}$ can be put in volumetric terms as,[13]

$$\left(\frac{\partial P}{\partial x_U}\right)^{\infty}_{T,\,\rho} = kT\rho^2(\bar{v}^{\infty}_{U}(SR) - v\bar{v}^{o}_{V}) \tag{6}$$

so that, the solvation driving-force can be interpreted macroscopically either in terms of the finite pressure perturbation $(\partial P/\partial x_U)^{\infty}_{T,\rho}$ as in Eq. (2), the finite volumetric perturbation $(\bar{v}^{\infty}_U(SR) - v\bar{v}^{o}_V)$, or the *effective* solvation number $N^{\infty}_{U,ex}(SR)$ as follows,

$$\mu^{r\infty}_U(T, P) - v\mu^{ro}_V(T, P) = kT \int_0^{\rho(P)} (\bar{v}^{\infty}_U(SR) - v\bar{v}^{o}_V)\, d\rho \tag{7}$$

and,

$$\mu^{r\infty}_U(T, P) - v\mu^{ro}_V(T, P) = kT \int_0^{\rho(P)} N^{\infty}_{U,ex}(SR) \frac{d\rho}{\rho} \tag{8}$$

The three quantities, $(\partial P/\partial x_U)^{\infty}_{T,\rho}$, $N^{\infty}_{U,ex}(SR)$, and $(\bar{v}^{\infty}_U(SR) - v\bar{v}^{o}_V)$ are measures of the so-called solute induced effects. In Section 2.4 we present the analogous expressions for the individual ions constituting the neutral salt.

## 2.1. Solubility Enhancement

In this section we use the formalism to establish the microscopic bases of the supercritical solubility enhancement in terms of molecular direct correlation function integrals. For example, the solubility equation for an incompressible pure non-volatile phase in equilibrium with a near-critical solvents reads,[19]

$$P\hat{\phi}_U x_U = f^s_U \approx \hat{\phi}^{sat}_U P^{sat}_U \exp[\beta v^s_U (P - P^{sat}_U)] \tag{9}$$

and the solubility enhancement factor becomes,[20]

$$E \equiv (x_U/x^{IG}_U) = (\hat{\phi}^{sat}_U/\hat{\phi}_U) \exp[\beta v^s_U (P - P^{sat}_U)] \tag{10}$$

where $x^{IG}_U = P^{sat}_U/P$, where $P^{sat}_U$, $v^s_U$, and $\hat{\phi}^{sat}_U$ are the vapor pressure, molar volume, and fugacity coefficient of the pure solute in the condensed phase at the prevailing state conditions, respectively. Thus, the enhancement factor can be finally recast as follows (see Appendix C of Chialvo and Cummings[7])

$$\begin{aligned} E \approx \hat{\phi}^{\infty}_U(T, P)^{-1} &= \hat{\phi}^{o}_V(T, P)^{-1} \exp\left[ -\int_0^{\rho(P)} \frac{\beta}{\rho^2} \left(\frac{\partial P}{\partial x_U}\right)^{\infty}_{T,\rho} d\rho \right] \\ &= \left(1 - v^o_V \int_0^{\rho(P)} C^o_{VV}\, d\rho\right) \exp\left(\int_0^{\rho(P)} C^{\infty}_{UV} \frac{d\rho}{\rho}\right) \end{aligned} \tag{11}$$

Equation (11) indicates the fundamental link between the solubility enhancement (decrease in $\hat{\phi}_U^{\infty}(T, P)$) and the local density perturbation around the solute (microstructure), and emphasizes two important issues. First, because Eq. (11) involves only short-ranged quantities, the increase in the solubility enhancement for attractive mixtures cannot be ascribed to the corresponding long-ranged increase in $\Gamma = \rho G_{UV}^{\infty} = 4\pi\rho \int_0^{\infty} (g_{UV}^{\infty}(r) - 1)\, r^2\, dr$ as proposed elsewhere.[10] Second, because small changes in the system pressure result in large changes in the solvent density in the near-critical region, Eq. (11) illustrates one of the advantages of near-critical processing: the solvation properties of the solvent can be modified significantly (and thus "tuned") through small changes in pressure.

## 2.2. Gas Solubility

Japas and Levelt Sengers[21] derived the limiting temperature dependence of Henry's constant and the solute distribution factor $K^{\infty}$ and presented two useful linear correlations for these quantities based on the so-called Krichevskii's parameter and the solvent's orthobaric density near the solvent's critical point. These expressions are,

$$T \ln K^{\infty} = \left(\frac{2}{k\rho_c^2}\right)\left(\frac{\partial P}{\partial x_U}\right)_{T_c, \rho_c}^{\infty} (\rho^l - \rho_c) \tag{12}$$

and

$$T \ln(H_{U,V}/f_V^o) = A + \left(\frac{1}{k\rho_c^2}\right)\left(\frac{\partial P}{\partial x_U}\right)_{T_c, \rho_c}^{\infty} (\rho^l - \rho_c) \tag{13}$$

where the constant $A \equiv T_c \ln[H_{U,V}(T_c)/f_V^o(T_c)]$ and $\rho^l$ is the orthobaric liquid density with a critical value $\rho_c$.[22] Even though these expressions were expected to be closely obeyed by real systems only in the neighborhood of the solvent's critical point, where the orthobaric path obeys the asymptotic expression $(v - v_c) = \pm |T - T_c|^{\beta - 1}$, these authors found that the linearity appeared to hold over a rather large orthobaric density range. However, the observed slopes do not show good agreement with the expected asymptotic values,[23] even though those from the $T \ln K^{\infty}$ vs. $(\rho^l - \rho_c)$ plots (Eq. (12)) are closer than those from $T \ln(H_{U,V}/f_V^o)$ vs. $(\rho^l - \rho_c)$ plots (Eq. (13)).

Wilhelm[24] later suggested that $T \ln L^{\infty}$ vs. $(\rho^l - \rho_c)$, where $L^{\infty} = (\rho^l/\rho^v)_{\sigma}/K^{\infty}$ is the Ostwald coefficient, rather than $T \ln K^{\infty}$ vs. $(\rho^l - \rho_c)$,

might result in a better linear relationship over a wider range of orthobaric densities. This suggestion was based on the fact that,

$$T \ln L^{\infty} = T \ln(\rho^l/\rho^v) - T \ln K^{\infty}$$
$$= T \ln([\rho_c + \Delta]/[\rho_c - \Delta]) - T \ln K^{\infty}, \qquad \Delta = \rho^l - \rho_c = \rho_c - \rho^v \tag{14}$$

after replacing $T \ln K^{\infty}$ in the right hand side of Eq. (14) by Eq. (12), and invoking the approximation $T \ln([\rho_c + \Delta]/[\rho_c - \Delta]) \approx 2T_c(\Delta/\rho_c)$ we obtain,

$$T \ln L^{\infty} = \left(\frac{2}{\rho_c}\right)\left[ T_c - \left(\frac{1}{k\rho_c}\right)\left(\frac{\partial P}{\partial x_U}\right)^{\infty}_{T_c, \rho_c}\right](\rho^l - \rho_c) \tag{15}$$

an expression that has the same asymptotic form as that for $T \ln K^{\infty}$ and $T \ln(H_{U,V}/f^o_V)$.

To test the orthobaric density dependence of $T \ln(H_{U,V}/f^o_V)$, $T \ln K^{\infty}$, and $T \ln L^{\infty}$, we invoke the following exact expressions,[21]

$$T \ln K^{\infty}(T) = T \lim_{x_U \to 0} \ln(y_U/x_U)$$
$$= (a^{r\infty}_x - a^{r\infty}_y)/k \tag{16}$$

and,

$$T \ln[H_{U,V}(T)/f^o_V(T)] = a^{r\infty}_x/k \tag{17}$$

Consequently,

$$T \ln L^{\infty} = T \ln(\rho^l/\rho^v) - (a^{r\infty}_x - a^{r\infty}_y)/k \tag{18}$$

with the derivative $a^{r\infty}_{\alpha} = (\partial a^r/\partial \alpha)^{\infty}_{T,\rho}$ given by (Appendix E of Chialvo *et al.*[25]),

$$a^{r\infty}_{\alpha} = \int_0^{\rho(P_\sigma)} \left(\frac{\partial P}{\partial \alpha_U}\right)^{\infty}_{T,\rho} \frac{d\rho}{\rho^2}, \qquad \alpha = x, y \tag{19}$$

where $x_U$ and $y_U$ denote the solute mole fractions in the liquid and vapor phase, respectively, $a^r = A^r/N$ is the residual Helmholtz free energy per molecule.

## 2.3. Solvation Effects on Kinetic Rate Constants in Supercritical Solvents

It has been suggested that the experimental isothermal kinetic rate constants of some reactions at near and supercritical conditions could not

be explained solely by the thermodynamic pressure effect. Some researchers have suggested that local composition enhancement and density augmentation effects around reactants are responsible for the lack of agreement between experimental kinetic rate constants measurements and predicted values by the transition state theory (TST) applied at the microscopic level using equations of state.[26–28]

Before accepting this explanation, it is worth noting that there are at least two other possible explanations for this lack of quantitative prediction of the pressure effects on the kinetic rates. First, the main players in the TST-approach, the species solvation properties, are *microscopic* quantities which, in macroscopic modeling, are indirectly described by *macroscopic* properties, which are difficult to measure or hard to predict accurately. Second, a frequently overlooked aspect is that the TST-approach relies on the hypothesis of unit transmission coefficient, i.e., no barrier re-crossing.[29] So unless we can address the real possibility of the breakdown of the TST while analyzing the experimental data, little can be said about the (lack of) agreement indicated above. We can address the first issue, through the application of the solvation formalism outlined in Section 2. With that purpose let us assume the following simple reaction,

$$\nu_R R + \nu_S S \overset{solvent}{\longleftrightarrow} \mathfrak{R}^{\ddagger} \rightarrow products \tag{20}$$

where $R$ is a solute reactant, $S$ is the cosolvent, $\mathfrak{R}^{\ddagger}$ is the activated complex in equilibrium with the reactants in solution, and the prefactors are the stoichiometry coefficients. Here we consider the case in which the cosolvents might participate in the reaction as reactants. According to the TST of reactions[29] the reaction rate constant is given by,

$$k^{TST} = \frac{kTK_0}{h} K_c^{\ddagger} \tag{21}$$

where $k$ and $h$ are Boltzmann and Planck constants, respectively, $T$ is the absolute temperature, $K_0$ is a factor that gives the correct units for $k^{TST}$, and $K_c^{\ddagger}$ is the molar based equilibrium constant for the activation process given by Eq. (20). In order to study the pressure effect on the kinetic rate constant we first rewrite $K_c^{\ddagger}$ in terms of the species fugacities, and then, determine the pressure coefficient of $\ln k^{TST}$ (see Appendix A of Chialvo *et al.*[30] for details),

$$\left(\frac{\partial \ln k^{TST}}{\partial P}\right)_{T,x} = -\Delta \nu \kappa + (\nu_R \bar{\upsilon}_R^{\infty} + \nu_S \bar{\upsilon}_S^{\infty} - \nu_{\mathfrak{R}} \bar{\upsilon}_{\mathfrak{R}}^{\infty})/kT \tag{22}$$

where $\Delta v^{\ddagger} = \nu_R \bar{\upsilon}_R^{\infty} + \nu_S \bar{\upsilon}_S^{\infty} - \nu_{\mathfrak{R}} \bar{\upsilon}_{\mathfrak{R}}^{\infty}$ is the actual activation volume.

Although Eq. (22) gives a macroscopic expression for the pressure derivative of the TST kinetic rate constant, it also allows us to introduce the solvation contributions in a precisely microscopic way. In fact, Eq. (22) can be rewritten as,[30]

$$\left(\frac{\partial \ln k^{TST}}{\partial P}\right)_{T,x} = \kappa\rho[\nu_R(\bar{v}_R^{\infty}(SR) - \bar{v}_R^{\infty(IG)}(SR) + \nu_S(\bar{v}_S^{\infty}(SR) - \bar{v}_S^{\infty(IG)}(SR) - \nu_{\mathfrak{R}}(\bar{v}_{\mathfrak{R}}^{\infty}(SR) - \bar{v}_{\mathfrak{R}}^{\infty(IG)}(SR))] \tag{23}$$

where $\rho = (1/\bar{v}_V^o)$ and the superscript *IG* denotes an ideal gas property. Thus, the pressure coefficient of the rate constant can be factorized into two terms, one involving the solvent's isothermal compressibility, and the other containing short-ranged solvation contributions to the species in solutions relative to their ideal gas contributions (absence of solute-solvent interactions). Note that the difference $(\bar{v}_U^{\infty}(SR) - \bar{v}_U^{\infty(IG)}(SR))$ actually subtracts the translational or "ideal gas" contribution from the $\bar{v}_U^{\infty}(SR)$, and therefore, contains only contributions from intermolecular interactions. Moreover, for reactions with $\Delta\nu = 0$, the "ideal gas" contributions cancel out, and the pressure effect becomes equal to the solvation contribution to the activation volume, $[\nu_R\bar{v}_R^{\infty}(SR) + \nu_S\bar{v}_S^{\infty}(SR) - \nu_{\mathfrak{R}}\bar{v}_{\mathfrak{R}}^{\infty}(SR)]$, magnified by the solvent's isothermal compressibility.

## 2.4. Ion Solvation

For the case of ionic solutes, the solvation analysis of Section 2 is still valid provided that $\nu = \nu_+ + \nu_-$, i.e., the solute species $U$ is the neutral salt, and therefore the properties of this hypothetical solute are linear combinations of the corresponding ion counterparts. In fact, for the case of ionic solutes the solvation process involves the perturbation of the solvent structure around the individual ions, and therefore, we can connect the solvent structure around each ion with properties of the hypothetical salt species. For example, the partial molar volume of the salt $U \equiv C^{\nu_+}A^{\nu_-}$ at infinite dilution becomes,

$$\bar{v}_U^{\infty} = \nu_-\bar{v}_-^{\infty} + \nu_+\bar{v}_+^{\infty} \tag{24}$$

where $\bar{v}_i^{\infty}$ is the partial molar volume of the ion $i$ at infinite dilution. Consequently,[13]

$$\left(\frac{\partial P}{\partial x_U}\right)_{T,\rho}^{\infty} = \nu_+\left(\frac{\partial P}{\partial x_+}\right)_{T,\rho}^{\infty} + \nu_-\left(\frac{\partial P}{\partial x_-}\right)_{T,\rho}^{\infty} \tag{25}$$

This expression indicates that the experimentally determined Krichevskii's parameter for electrolyte solutions[18, 31] is actually a linear combination of those corresponding to the individual ions forming the salt, i.e.,

$$\left(\frac{\partial P}{\partial x_i}\right)^{\infty}_{T,\rho} = kT\rho(C^{o}_{VV} - C^{\infty}_{iV} - T^{\infty}_{iV}); \qquad i = +, - \tag{26}$$

which can also be written in two equivalent forms,[32]

$$\left(\frac{\partial P}{\partial x_i}\right)^{\infty}_{T,\rho} = kT\rho(\bar{v}^{\infty}_{i}(SR) - \bar{v}^{o}_{V}); \qquad i = +, - \tag{27}$$

and,

$$\left(\frac{\partial P}{\partial x_i}\right)^{\infty}_{T,\rho} = -\frac{N^{\infty}_{i,ex}(SR)}{\kappa^{IG}}; \qquad i = +, - \tag{28}$$

where $\bar{v}^{\infty}_{i}(SR)$ and $N^{\infty}_{i,ex}(SR)$ are the individual-ion counterparts of $\bar{v}^{\infty}_{U}(SR)$ and $N^{\infty}_{U,ex}(SR)$,[32] respectively. $T^{\infty}_{iV}$ is a solvent property[33] given by,

$$T^{\infty}_{iV} = -\frac{4\pi\rho q_i(\varepsilon - 1)}{3\varepsilon\mu}\int_0^{\infty} r^3 c^{101}_{00;\,VV}(r)\, dr \tag{29}$$

where $\varepsilon$ is the solvent dielectric constant, $q_i$ is the ion charge, $\mu$ is the solvent's dipole moment, and $c^{101}_{00;\,VV}(r)$ is the $r$-dependent (101) coefficient of the rotational invariant expansion of the solvent-solvent direct correlation function.[34]

Note finally that the above equations for the ions allows us to define the solvation thermodynamics of the individual ions constituting the neutral ionic solute, in terms of the corresponding ion-induced effects by replacing $(\partial P/\partial x_i)^{\infty}_{T,\rho}$ with the corresponding expressions (26)–(28),

$$\begin{aligned}\mu^{r\infty}_{i}(T, P) - \mu^{ro}_{V}(T, P) &= \int_0^{\rho(P)} \left(\frac{\partial P}{\partial x_i}\right)^{\infty}_{T,\rho} \frac{d\rho}{\rho^2} \\ &= kT\ln[\hat{\phi}^{\infty}_{i}/\hat{\phi}^{o}_{V}]; \qquad i = -, +\end{aligned} \tag{30}$$

so that, from Eq. (1), we have

$$\mu^{r\infty}_{U}(T, P) - \nu\mu^{ro}_{V}(T, P) = \nu kT\ln(\hat{\phi}^{\infty}_{U}/\hat{\phi}^{o}_{V}) \tag{31}$$

with $(\hat{\phi}^{\infty}_{U})^{\nu} = (\hat{\phi}^{\infty}_{+})^{\nu_+}(\hat{\phi}^{\infty}_{-})^{\nu_-}$, where $\hat{\phi}^{\infty}_{i}$ is the partial molar fugacity coefficient for the individual ion $i$ at infinite dilution.

## 3. SOME TYPICAL RESULTS

Here we use the Ornstein-Zernike integral equations with the adequate closure approximations to determine the pair correlation functions, their integrals, and the thermodynamic properties of the infinitely dilute systems of interest.

### 3.1. Solubility Enhancement

In this section we present some results for the solvation behavior of two near-critical Lennard-Jones binary mixtures which have been studied previously by molecular dynamics simulation. They are the infinitely dilute solutions of pyrene in near-critical carbon dioxide[35, 36] and di-*ter*-butylnitroxide (*DTBN*) in near-critical ethane.[37] According to the classification of Debenedetti and Mohamed,[38] these mixtures are usually referred to as attractive systems ($C^{\infty}_{UV} > 1$) which in macroscopic terms means a non-volatile solute ($(\partial P/\partial x_U)^{\infty}_{T,\rho} < 0$).[8] For the sake of comparison we have studied the density dependence ($0.05 \leqslant \rho\sigma^3_V \leqslant 0.5$) of the microscopic and macroscopic properties of these three systems at the same reduced temperature $T_r = 1.02$.

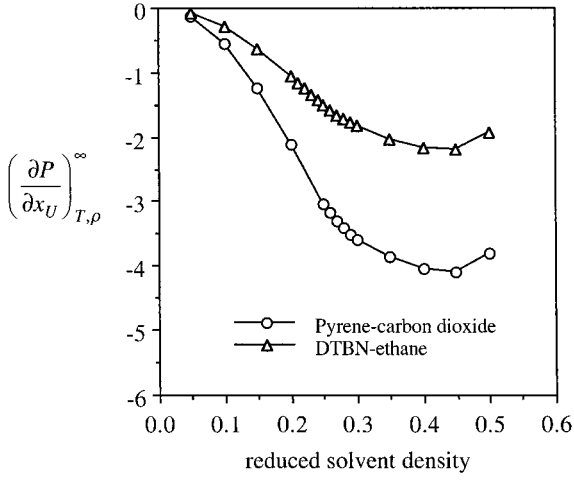


Fig. 1. Comparison between the density dependence of $(\partial P/\partial x_U)^{\infty}_{T,\rho}$ for the attractive Lennard-Jones pyrene(U)-$CO_2$(V) and *DTBN*(U)-ethane(V) systems at $T_r = T/T_c = 1.02$ from PY calculations. All quantities are reduced in terms of the solvent's Lennard-Jones parameters.

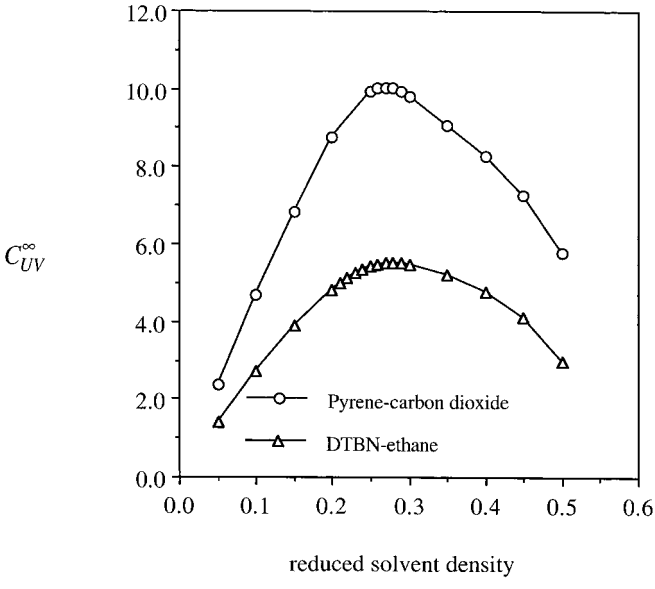


Fig. 2. Comparison between the density dependence of $C_{UV}^{\infty}$ for the attractive Lennard-Jones pyrene(U)-$CO_2$(V) and *DTBN*(U)-ethane(V) systems at $T_r = T/T_c = 1.02$ from PY calculations. All quantities are reduced in terms of the solvent's Lennard-Jones parameters.

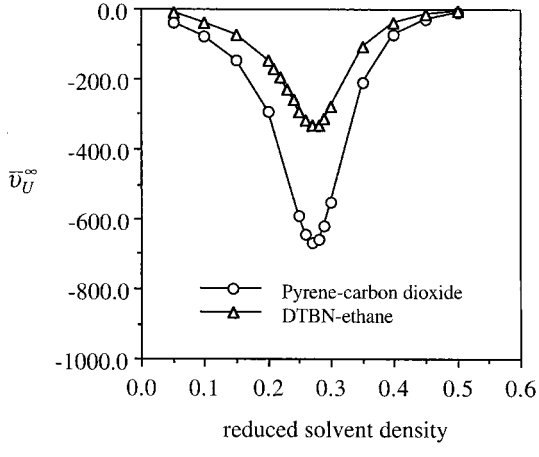


Fig. 3. Comparison between the density dependence of $\bar{v}_U^{\infty}$ for the attractive Lennard-Jones pyrene(U)-$CO_2$(V) and *DTBN*(U)-ethane(V) systems at $T_r = T/T_c = 1.02$ from PY calculations. All quantities are reduced in terms of the solvent's Lennard-Jones parameters.

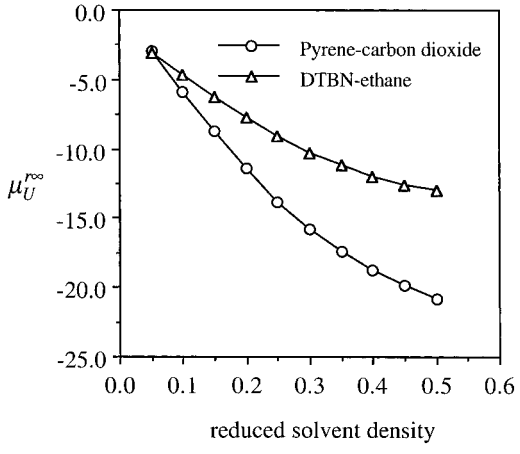


Fig. 4. Comparison between the density dependence of $\mu_U^{r\infty}$ for the attractive Lennard-Jones pyrene(U)-$CO_2$(V) and *DTBN*(U)-ethane(V) systems at $T_r = T/T_c = 1.02$ from PY calculations. All quantities are reduced in terms of the solvent's Lennard-Jones parameters.

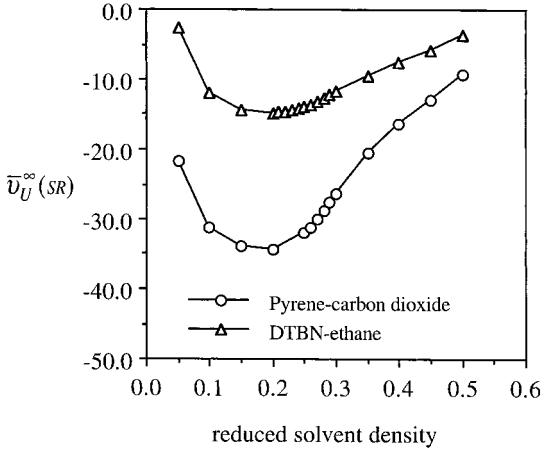


Fig. 5. Comparison between the density dependence of $\bar{v}_U^{\infty}(SR)$ for the attractive Lennard-Jones pyrene(U)-$CO_2$(V) and *DTBN*(U)-ethane(V) systems at $T_r = T/T_c = 1.02$ from PY calculations. All quantities are reduced in terms of the solvent's Lennard-Jones parameters.

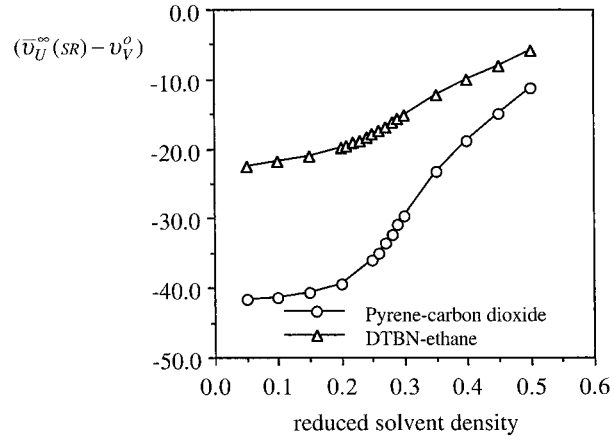


Fig. 6. Comparison between the density dependence of $(\bar{v}_U^{\infty}(SR) - \bar{v}_V^o)$ for the attractive Lennard-Jones pyrene(U)-$CO_2$(V) and *DTBN*(U)-ethane(V) systems at $T_r = T/T_c = 1.02$ from PY calculations. All quantities are reduced in terms of the solvent's Lennard-Jones parameters.

All systems are modeled as Lennard-Jones spheres with potential parameters given in Tables 1 and 2 of Chialvo and Cummings.[7] Results in Figs. 1 and 2 confirm unambiguously that pyrene and *DTBN* in supercritical $CO_2$ and ethane, respectively, involve attractive solute-solvent interactions, i.e., $(\partial P/\partial x_U)_{T,\rho}^{\infty} < 0$ and $C_{UV}^{\infty} > 1$, being the pyrene-$CO_2$ system

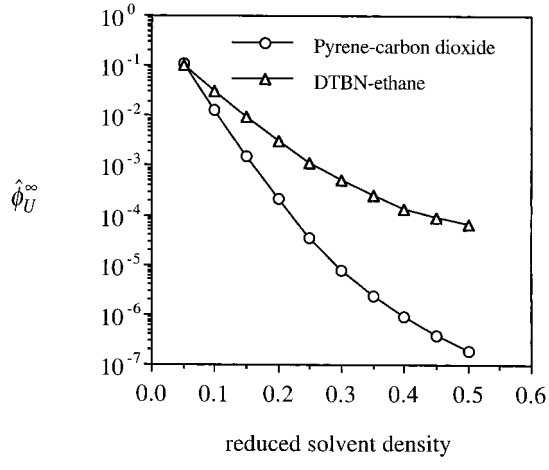


Fig. 7. Comparison between the density dependence of $\hat{\phi}_U^{\infty}$ for the attractive Lennard-Jones pyrene(U)-$CO_2$(V) and *DTBN*(U)-ethane(V) systems at $T_r = T/T_c = 1.02$ from PY calculations. All quantities are reduced in terms of the solvent's Lennard-Jones parameters.

slightly more attractive than the *DTBN*-ethane as we would expect according to the relative sizes of the corresponding Lennard-Jones parameters. This is also clearly reflected in the sign (negative) of the corresponding solute's partial molar volumes (Fig. 3), and solute's residual chemical potentials (Fig. 4).

In Fig. 5 we compare the density dependence for the short-ranged contribution to the solute's partial molar volume $\bar{v}_U^{\infty}(SR)$. For both mixtures the density dependence of $\bar{v}_U^{\infty}(SR)$ shows a minimum at $\rho\sigma_V^3 < \rho_c\sigma_V^3 = 0.28$, $\bar{v}_U^{\infty}(SR)$ being more negative for the pyrene-$CO_2$ system. However, the density dependence of the solute-induced local effect on the solvent's local density $(\bar{v}_U^{\infty}(SR) - v_V^o)_{T,\rho}$ (Fig. 6) shows only a change of curvature around $\rho\sigma_V^3 < \rho_c\sigma_V^3 = 0.18$. Note also that even though $\mu_U^{r\infty}$ presents a moderate density dependence (it changes by a factor of 2-3 for $0.05 \leqslant \rho\sigma_V^3 \leqslant 0.5$), $\hat{\phi}_U^{\infty}$ (Fig. 7) shows extreme sensitivity to density, exhibiting a 3-6 orders of magnitude change in the same density range.

## 3.2. Gas Solubility

In this section we analyze the density dependence of $a_\alpha^{r\infty} = (\partial a^r/\partial\alpha)_{T,\rho}^{\infty}$, by considering the thermodynamic behavior of an infinitely dilute solution of *Ne* along the coexistence curve of the solvent, *Xe*, and extract some important information about the orthobaric density dependence of $(\partial P/\partial x_U)_{T,\rho}^{\infty}$ in the vicinity of and away from the solvent's critical point. The system is modeled as a two-component hard-core Yukawa fluid (HCYF), for which the intermolecular potential $\phi_{ij}(r)$ is,

$$\phi_{ij}(r) = \begin{cases} \infty & \text{if} \quad r < \sigma_{ij} \\ \omega_{ij}(r) & \text{if} \quad r > \sigma_{ij} \end{cases} \tag{31}$$

where $\sigma_{ij}$ is the hard-sphere diameter for the *ij*-interaction, and

$$\omega_{ij}(r) = -\frac{\varepsilon_{ij}\sigma_{ij}}{r}\exp(-\alpha_{ij}(r-\sigma_{ij})) \tag{32}$$

Following Henderson *et al.*[39] we choose $\alpha_{ij}\sigma_{ij} = 1.8$ for all *ij*-pairs.

The rationale behind this choice is twofold: despite its simplicity this model shows a vapor-liquid phase transition and, within the mean spherical approximation (MSA) closure, this model offers an analytical solution to the Ornstein-Zernike equation.[40] The MSA is known to be quite reliable in predicting thermodynamic properties of Yukawa fluids.[39, 41] In particular, the phase envelope for the LJ fluid can be described by the MSA for the corresponding HCYF.[42] The integral equation calculations

must be carried out using a theory which is able to provide a consistent description of both the structure and the thermodynamics in the vicinity of the solvent's critical point. By consistency we mean that the critical point of the liquid-vapor coexisting curve, obtained from the condition of equal chemical potentials and pressure in both phases, should coincide with the critical point of the spinodal line defined by the condition $\beta(\partial P/\partial \rho)_T = 1 - \rho \hat{c}(\mathbf{0}) = 0$.

To achieve this consistency we have chosen to use the generalized MSA (GMSA) which for the present two-component system reads,

$$\begin{cases} c_{ij}(r) = -\beta\omega_{ij}(r) + r^{-1} \sum_{n=1}^{N} A_{ij}^{(n)} \exp(-z_{ij}^{(n)} r) & \text{if} \quad r > \sigma_{ij} \\ h_{ij}(r) = -1 & \text{if} \quad r < \sigma_{ij} \end{cases} \tag{33}$$

where the Yukawa terms are introduced to correct the regular MSA for thermodynamic self-consistency. If the contact values of the radial distribution functions $g_{ij}(r)$) and the isothermal compressibility are known, then the method of Høye and Stell[43] can be used to determine the Yukawa coefficients in Eq. (33) which will enforce thermodynamic consistency. In the present study we consider an infinitely dilute solution, which means that the correction is only done for the solvent-solvent correlation, and, for simplicity, we truncate the summation of Yukawa terms at $N = 2$, with $\sigma_{11} z_{11}^{(1)} = 9$ and $\sigma_{11} z_{11}^{(2)} = 16$. The parameters $A_{11}^{(n)}$ $(n = 1, 2)$ follow from the solution of the constraints imposed on the contact values of the pair correlation functions and the isothermal compressibility, i.e., the condition of thermodynamic consistency. One way to do this is by means of an equation of state derived via the MSA energy route[43] which yields quite accurate thermodynamics. However, again for the sake of simplicity, here we have used the thermodynamic results from a perturbation theory presented elsewhere.[39] In order to satisfy the ideal solution condition, i.e., for which solute-solute, solute-solvent and solvent-solvent potential parameters and consequently the equality of species chemical potentials, in a previous work[44] we assumed the convenient though arbitrary condition for the Yukawa parameters,

$$\begin{aligned} \sigma_{ij} z_{ij}^{(n)} &= \sigma_{11} z_{11}^{(n)} \\ A_{ij}^{(n)} &= \frac{\varepsilon_{ij}\sigma_{ij}}{\varepsilon_{11}\sigma_{11}} A_{11}^{(n)} \end{aligned} \tag{34}$$

However, for large solute-solvent molecular asymmetry as is usually found in gas solvation, the GMSA closure for solute-solvent correlations does not

guarantee accurate results. Therefore, in the present case we assume the regular MSA closure for the solute-solvent correlations, since it is known to yield reasonably accurate thermodynamics.[39, 41, 45] Our choice is supported by the fact that here we are studying systems with large solute-solvent asymmetries.

In order to calculate the chemical potential along the liquid branch of the phase envelope we need to perform an integration, Eq. (19), across the two-phase region. Since our GMSA does not give real solutions in this region, we perform the integration by means of the method proposed by Ebner *et al.*[45] In these studies a similar integration is performed by interpolating the values of the direct correlation functions corresponding to the orthobaric conditions. Since the solution of the GMSA is available in the entire range of temperature and density, except for a rather small region between the spinodal lines, this interpolation is sufficiently accurate for our purposes.

The solution of the GMSA with the Yukawa coefficients as defined in Eq. (34) is obtained by the Baxter factorization method.[46] The general scheme of the solution is similar to that presented elsewhere.[47, 48] In the present case the analytical solution results in a set of non-linear algebraical equations for the Yukawa parameters $A_{11}^{(n)}$ together with the parameters related to the Baxter factorization functions. We solve this set of equations by an iterative approach as described by Kalyuzhnyi and Holovko.[49] In summary, this formalism gives a self-consistent description of both thermodynamics and microstructure for the model in the entire region of state conditions of interest.

In Fig. 8 we show the vapor-liquid coexistence curve for the pure solvent, described as a hard-core Yukawa fluid. Note that the binodal and spinodal curves meet at the critical conditions, i.e., $kT_c/\varepsilon_{VV}=1.256$ and $\rho_c\sigma_{VV}^3=0.313$ where $\sigma_{11}=\sigma_{VV}$ and $\varepsilon_{11}=\varepsilon_{VV}$ are the solvent's size and energy parameters. In what follows we study an infinitely dilute solute $U\equiv Xe$ in a solvent $V\equiv Ne$ characterized by a ratio of size parameters $(\sigma_{UU}/\sigma_{VV})=0.697$ and a ratio of energy parameters $(\varepsilon_{UU}/\varepsilon_{VV})=0.142$. This asymmetry corresponds to the system $Ne(V)-Xe(U)$ if described as Lennard-Jones spheres.[7]

The orthobaric density dependence of $(\partial P/\partial x_U)_{T,\rho}^{\infty}$ for this infinitely dilute mixture is shown in Fig. 9. In order to understand how the two asymmetries contribute to the nonideality, we compare the original system $(\sigma_{UU}/\sigma_{VV})=0.697$ and $(\varepsilon_{UU}/\varepsilon_{VV})=0.142$ with two special cases; one in which $\sigma_{UU}=\sigma_{VV}$ and $\varepsilon_{UU}=0.142\varepsilon_{VV}$, and the other in which $\sigma_{UU}=0.697\sigma_{VV}$ and $\varepsilon_{UU}=\varepsilon_{VV}$. According to the results of Fig. 9 the change on the solute's size and energy parameters, $\sigma_{UU}$ and $\varepsilon_{UU}$, shows opposite effects on the orthobaric density dependence of $(\partial P/\partial x_U)_{T,\rho}^{\infty}$. Compensation

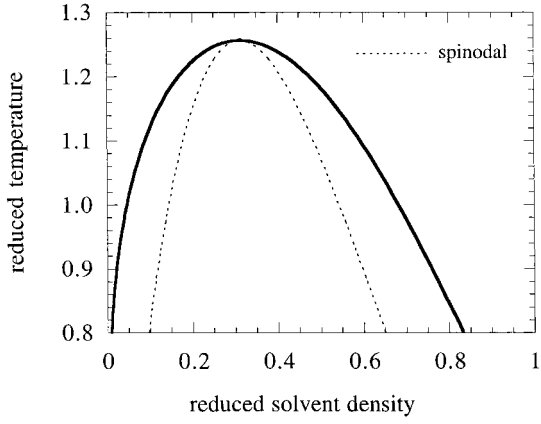


Fig. 8. Phase envelope of a hard-core Yukawa fluid with $\alpha_{11}\sigma_{11} = 1.8$ as predicted by the integral equation calculations. All quantities are reduced in terms of the solvent parameters $\varepsilon_{VV}$ and $\sigma_{VV}$.

between nonidealities originated from energy and size asymmetries has been already observed for other model systems[50, 51] and, in this case, it may explain the observed quasi-linearity on the orthobaric density dependence of $(\partial P/\partial x_U)^{\infty}_{T,\rho}$. For the system of interest, $(\sigma_{UU}/\sigma_{VV}) = 0.697$ and $(\varepsilon_{UU}/\varepsilon_{VV}) = 0.142$, Krichevskii's parameter $(\partial P/\partial x_U)^{\infty}_{T_c,\rho_c} = 0.6246\varepsilon_{VV}/\sigma^3_{VV}$.

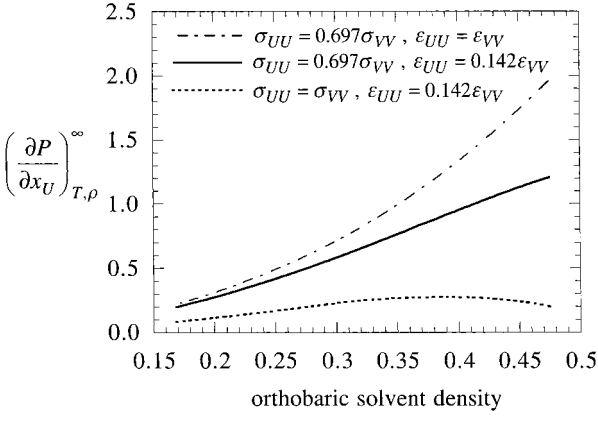


Fig. 9. Comparison between the orthobaric density dependence of $(\partial P/\partial x_U)^{\infty}_{T,\rho}$ for three repulsive infinitely dilute hard-core Yukawa fluid mixtures with $\alpha_{11}\sigma_{11} = 1.8$. The coefficients indicate the relative sizes of $\sigma_{UU}$ and $\varepsilon_{UU}$ with respect to the solvent's parameters. All quantities are reduced in terms of the solvent parameters $\varepsilon_{VV}$ and $\sigma_{VV}$.

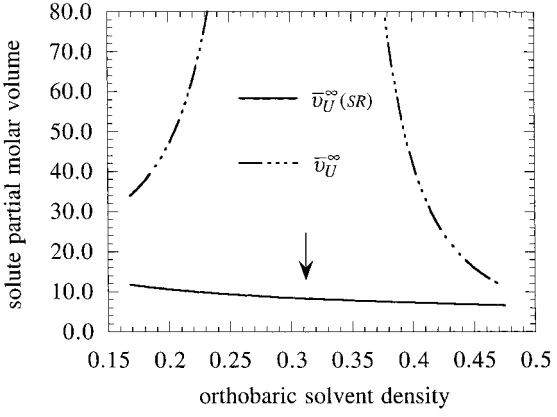


Fig. 10. Orthobaric density dependence of the infinite dilute solute partial molar volume $\bar{v}_U^{\infty}$ for the infinitely dilute hard-core Yukawa system with $\alpha_{11}\sigma_{11} = 1.8$, $(\sigma_{UU}/\varepsilon_{VV}) = 0.697$, and $(\varepsilon_{UU}/\varepsilon_{VV}) = 0.142$. Comparison between the total (SR + LR) and the short-range (SR) contributions. Arrow indicates the location of the solvent's critical density. All quantities are reduced in terms of trhe solvent parameters $\varepsilon_{VV}$ and $\sigma_{VV}$.

In Fig. 10 we show the comparison between the behavior of the infinitely dilute solute partial molar volume, $\bar{v}_U^{\infty}$, and its corresponding short-range ($SR$) contribution, $\bar{v}_U^{\infty}(SR)$, along the coexistence curve of pure solvent as predicted by the integral equation calculations. These properties are positive, the solute-solvent asymmetry gives rise to a volatile solute characterized macroscopically by $(\partial P/\partial x_U)_{T,\rho}^{\infty} > 0$ (Fig. 9), and microscopically by a relative depletion of the local density of solvent around the solute with respect to that around any solvent molecule. Note that while $\bar{v}_U^{\infty}$ shows the typical compressibility-driven divergence at the solvent's critical point, $\bar{v}_U^{\infty}(SR)$ behaves smoothly along the coexistence curve.

In Fig. 11 we display the predicted orthobaric density dependence of $a_{\alpha}^{r\infty}$, Eq. (19). Note that this property shows an almost linear behavior along the entire density domain, a prelude of similar behavior for the related solvation quantities. For example, in Figs. 12 and 13 we present the corresponding behavior for Henry's constant and solute distribution factor along the liquid branch of the coexistence curve. The slopes of the $T \ln K^{\infty}$ vs. $\rho^l$ and $T \ln(H_{U,V}/f_V^o)$ vs. $\rho^l$ representations are $12.092\varepsilon_{VV}\sigma_{VV}^3/k$ and $6.352\varepsilon_{VV}\sigma_{VV}^3/k$, respectively, with a correlation coefficient greater than 0.9998. If we assume the asymptotic expressions (12) and (13), then these slopes predict $0.592\varepsilon_{VV}/\sigma_{VV}^3$ and $0.622\varepsilon_{VV}/\sigma_{VV}^3$ for Krichevskii's parameters, respectively, in comparison to the actual value of $0.625\varepsilon_{VV}/\sigma_{VV}^3$, i.e., within a 5% range.

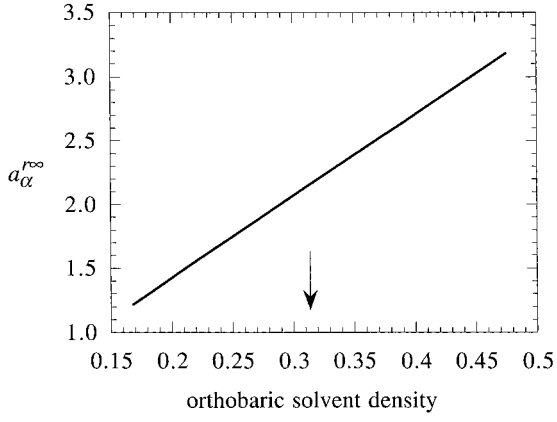


Fig. 11. Orthobaric density dependence of $a_\alpha^{r\infty} = (\partial a^r/\partial \alpha_U)_{T,\rho}^{\infty}$ for the infinitely dilute hard-core Yukawa system with $\alpha_{11}\sigma_{11} = 1.8$, $(\sigma_{UU}/\sigma_{VV}) = 0.697$, and $(\varepsilon_{UU}/\varepsilon_{VV}) = 0.142$. Arrow indicates the location of the solvent's critical density. All quantities are reduced in terms of the solvent parameters $\varepsilon_{VV}$ and $\sigma_{VV}$.

Regarding the behavior of Ostwald's coefficient $L^\infty$, Fig. 14, the fact that the two contributions to $T \ln L^\infty$, $T \ln K^\infty$ and $T \ln(\rho^l/\rho^v)_\sigma$, show opposite density dependence gives support to Wilhelm's suggestion that $T \ln L^\infty$ vs. $(\rho^l - \rho_c)$, may show a better linear relationship than $T \ln K^\infty$ vs. $(\rho^l - \rho_c)$ in a wider range of orthobaric densities.[24] For our model system, both $T \ln K^\infty$ and $T \ln(\rho^l/\rho^v)_\sigma$ present linear dependence with $\rho^l$

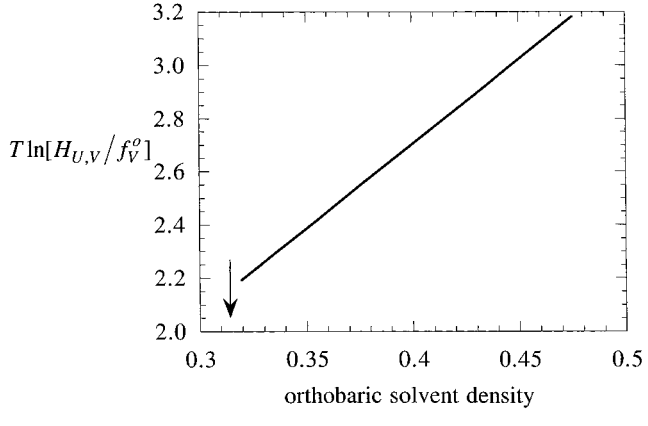


Fig. 12. Orthobaric density dependence of $T \ln(H_{U,V}/f_V^o)$ for the infinitely dilute hard-core Yukawa system with $\alpha_{11}\sigma_{11} = 1.8$, $(\sigma_{UU}/\sigma_{VV}) = 0.697$, and $(\varepsilon_{UU}/\varepsilon_{VV}) = 0.142$. Arrow indicates the location of the solvent's critical density. All quantities are reduced in terms of the solvent parameters $\varepsilon_{VV}$ and $\sigma_{VV}$.

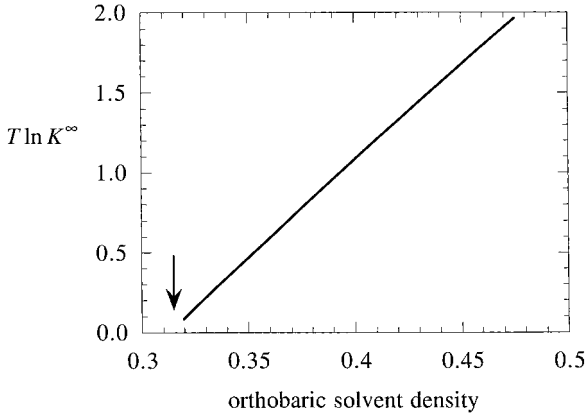


Fig. 13. Orthobaric density dependence of $T \ln K^{\infty}$ for the infinitely dilute hard-core Yukawa system with $\alpha_{11}\sigma_{11} = 1.8$, $(\sigma_{UU}/\sigma_{VV}) = 0.697$, and $(\varepsilon_{UU}/\varepsilon_{VV}) = 0.142$. Arrow indicates the location of the solvent's critical density. All quantities are reduced in terms of the solvent parameters $\varepsilon_{VV}$ and $\sigma_{VV}$.

with correlation factors larger than 0.9997. Therefore, it is not likely under this circumstance to observe any improvement in the linear regression of $T \ln L^{\infty}$ vs. $\rho^l$ over the other solvation quantities.

If we assume Eq. (15) to be also valid beyond the asymptotic region, based on the observed linear behavior of $T \ln K^{\infty}$ and $T \ln(\rho^l/\rho^v)_{\sigma}$ vs. $\rho^l$

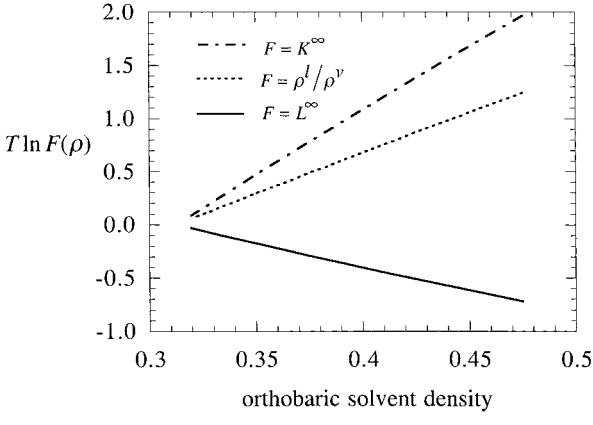


Fig. 14. Orthobaric density dependence of $T \ln F$, $F = K^{\infty}$, $\rho^l/\rho^v$, $L^{\infty}$, for the infinitely dilute hard-core Yukawa system with $\alpha_{11}\sigma_{11} = 1.8$, $(\sigma_{UU}/\sigma_{VV}) = 0.697$, and $(\varepsilon_{UU}/\varepsilon_{VV}) = 0.142$. Arrow indicates the location of the solvent's critical density. All quantities are reduced in terms of the solvent parameters $\varepsilon_{VV}$ and $\sigma_{VV}$.

for our model system, then the regressed Krichevskii's parameter is $(\partial P/\partial x_U)^{\infty}_{T_c,\rho_c} = 0.610\varepsilon_{VV}/\sigma^3_{VV}$, i.e., between those obtained by regression of $T \ln K^{\infty}$ and $T \ln(H_{U,V}/f^o_V)$.

## 3.3. Solvation Effects on Kinetic Rate Constants

In this section we illustrate the solvation behavior of Lennard-Jones mixtures composed of a solvent and three infinitely dilute species, one of them being a cosolvent. While the Lennard-Jones model provides a pedestrian representation of the actual reacting systems studied by Roberts *et al.*[52] they allow us to illustrate the effect of species-solvent molecular asymmetry on the pressure dependence of the kinetic rate constants. The system under consideration consists of triplet benzophenone ($^3BP$) as an infinitely dilute reactant, either $O_2$ or 1,4-cyclohexadiene as an infinitely dilute reactive cosolvent, the infinitely dilute transition state species ($TS$), all immersed in supercritical solvent $CO_2$.

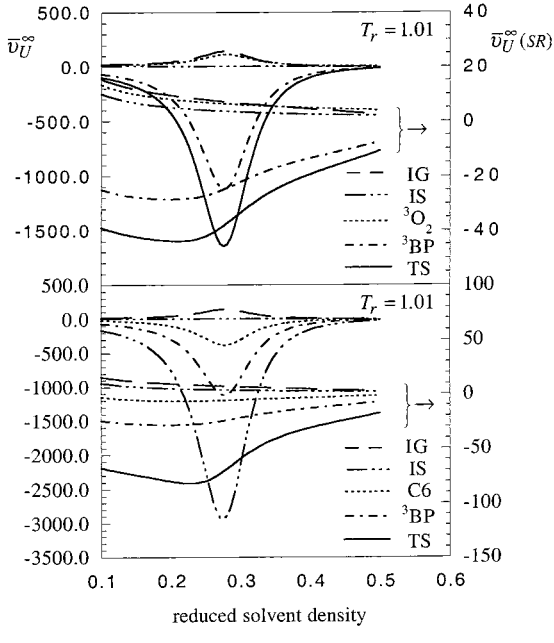


Fig. 15. Density dependence of species partial molar volume $\bar{v}_U^{\infty}$ and its solvation counterpart $\bar{v}_U^{\infty}(SR)$ at $T_r = 1.01$ for the reactive systems $^3BP + {}^3O_2 + CO_2 \Leftrightarrow TS$ (upper), and $^3BP + 1,4\_C_6 + CO_2 \Leftrightarrow TS$ (lower). All quantities are reduced in terms of the solvent parameters $\varepsilon_{VV}$ and $\sigma_{VV}$.

Because of the central role played by the partial molar volume of species in solution, we first determine their density dependence for the three species at infinite dilution along the near-critical isotherm $T_r = 1.01$ as shown in Figs. 15a, b in comparison with the corresponding $\bar{v}_U^{\infty}(SR)$. [Note that because 100 volume units $\approx 2.0$ liter/mol in these illustrations, the species partial molar volumes at near-critical conditions vary from 3.0 liter/mol (oxygen) to $-30$ liter/mol (transition state complex). In contrast, the corresponding solvation contributions go from 0.15 liter/mol to 1.45 liter/mol]. For illustration purposes, we have also included in these graphs the properties of two limiting cases, a *solute* in the ideal solution (*IS*), i.e., the pure solvent, and the ideal gas solute (*IG*). These cases are very convenient references because they encompass two extreme molecular asymmetries, i.e., the presence of intermolecular forces with no solute-solvent asymmetry, and the absence of solute-solvent interactions, respectively.

As the solute becomes less repulsive, with respect to that of an ideal gas (see Appendix A of Chialvo *et al.*[30]), $(\partial P/\partial x_U)^{\infty}_{T,\rho,x_{k\neq u}}$ reaches zero for

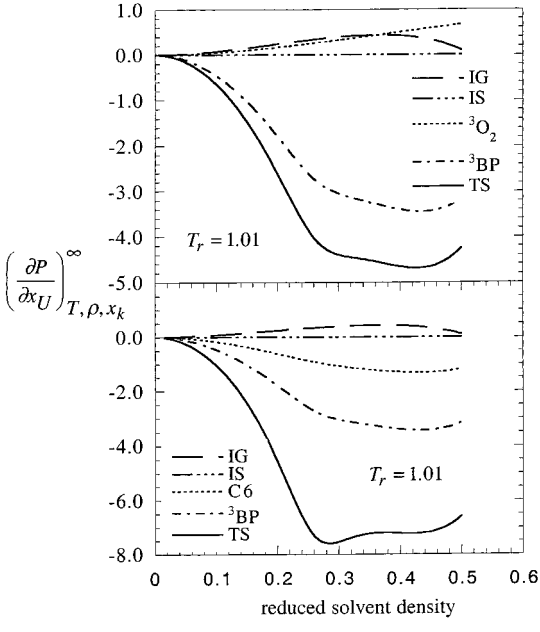


Fig. 16. Density dependence of species $(\partial P/\partial x_U)^{\infty}_{T,\rho,x_{k\neq u}}$ at $T_r = 1.01$ for the reactive system $^3BP + {}^3O_2 + CO_2 \Leftrightarrow TS$ (upper) and $^3BP + 1{,}4\_C_6 + CO_2 \Leftrightarrow TS$ (lower). All quantities are reduced in terms of the solvent parameters $\varepsilon_{VV}$ and $\sigma_{VV}$.

the ideal solution (*IS*), and then becomes negative for the more pronounced molecular asymmetries (see Figs. 16a, b). Note that this function can show an extreme finite value at a density greater or smaller than the critical, depending on the molecular asymmetry, with the exception of the *IS* for which $(\partial P/\partial x_U)^{\infty}_{T,\rho,x_{k\neq u}} = 0$ at any state condition. Correspondingly, the partial molar volumes $\bar{v}^{\infty}_U$ becomes less positive as we turn on the molecular interactions ($IG \rightarrow IS$), and reaches large negative values as we increase the molecular asymmetry with respect to the solvent. In all cases, except for the *IS*, $\bar{v}^{\infty}_U$ exhibits an extreme value around the density where the isothermal compressibility does. In contrast, $\bar{v}^{\infty}_U(SR)$ shows positive values with a monotonic density change for the *IG* and *IS* cases. Then, for more pronounced asymmetries, $\bar{v}^{\infty}_U(SR)$ exhibits a positive extreme depending on the behavior of $(\partial P/\partial x_U)^{\infty}_{T,\rho,x_{k\neq u}}$.

The positive partial molar volume at infinite dilution exhibited by the oxygen, the signature of a volatile, $(\partial P/\partial x_U)^{\infty}_{T,\rho,x_{k\neq u}} > 0$,[8] or repulsive[38] solute is the expected behavior for a dissolved gas in a near-critical solvent. In contrast, the 1,4-*cyclohexadiene*, the triplet benzophenone and the

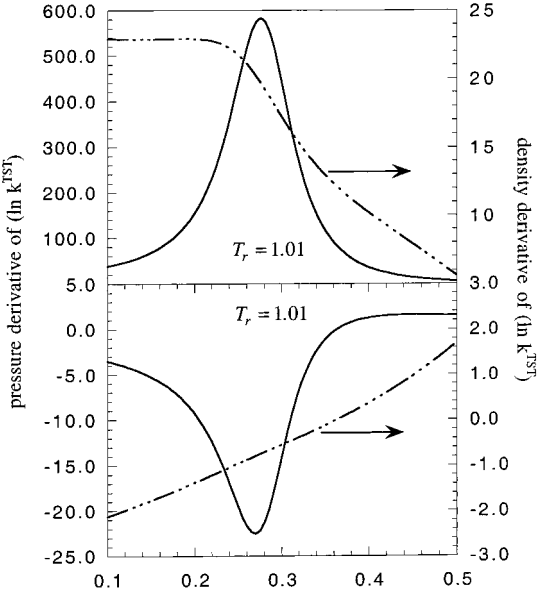


Fig. 17. Comparison between $(\partial \ln k^{TST}/\partial P)_{T,x}$ and $(\partial \ln k^{TST}/\partial \rho)_{T,x}$ for the reactive system ${}^3BP + {}^3O_2 + CO_2 \Leftrightarrow TS$ and at $T_r = 1.01$ and $\rho_r = 1.0$, with $(\xi = (\varepsilon_{UV}/\varepsilon^B_{UV}) = 1.0,\ \eta = (\sigma_{UV}/\sigma^L_{UV}) = 1.0)$ (upper), and $(\xi = (\varepsilon_{UV}/\varepsilon^B_{UV}) \approx 0.94,\ \eta = (\sigma_{UV}/\sigma^L_{UV}) \approx 0.93)$ (lower).

corresponding transition state complexes ($TS$) exhibit the typical non-volatile, $(\partial P/\partial x_U)^{\infty}_{T,\rho,x_{k\neq u}} < 0$, or attractive behavior usually associated with bulky (strongly interacting) solutes. This behavior can be clearly seen in Figs. 16a, b where we display the corresponding density dependence for $(\partial P/\partial x_U)^{\infty}_{T,\rho,x_{k\neq u}}$, the macroscopic quantity that most succinctly characterizes the solvation phenomenon.

The dependence of the sign of the $(\partial \ln k^{TST}/\partial P)_{T,x}$ on the relative asymmetries between solute species and the solvent becomes more evident when considering the sensitivity of the solvation properties to perturbations of the solute-solvent interactions (e.g., combining rules). Since we have used the Lorentz and Berthelot rules throughout our calculations ($\varepsilon^B_{UV} = (\varepsilon_{VV}\varepsilon_{UU})^{0.5}$ and $\sigma^L_{UV} = 0.5(\sigma_{VV}+\sigma_{UU})$), and our earlier investigation indicated that small perturbations of these rules have profound effects on the corresponding excess properties,[53] we decided to study their effect on the resulting $(\partial \ln k^{TST}/\partial P)_{T,x}$. For example, a 4% decrease from the Berthelot rule, $\xi = (\varepsilon_{UV}/\varepsilon^B_{UV}) \approx 0.96$, and a 7% decrease from the Lorentz rule, $\eta = (\sigma_{UV}/\sigma^L_{UV}) \approx 0.93$, for the $TS - CO_2$ interactions suffices to match

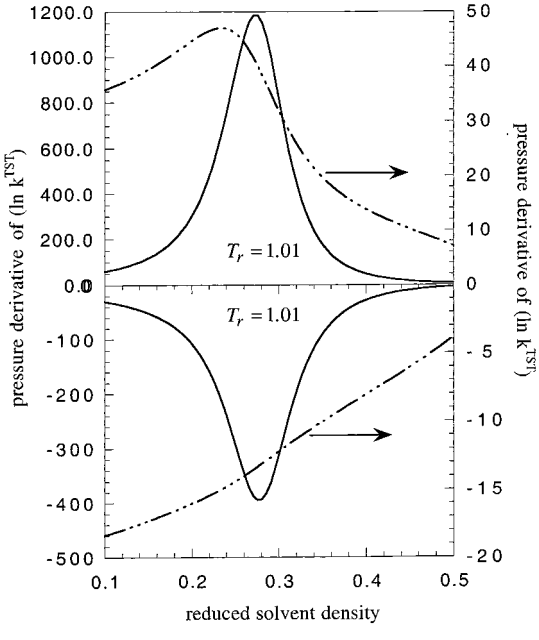


Fig. 18. Comparison between $(\partial \ln k^{TST}/\partial P)_{T,x}$ and $(\partial \ln k^{TST}/\partial \rho)_{T,x}$ for the reactive system ${}^3BP + 1,4\_C_6 + CO_2 \Leftrightarrow TS$ and at $T_r = 1.01$ and $\rho_r = 1.0$, with ($\xi = (\varepsilon_{UV}/\varepsilon^B_{UV}) = 1.0$, $\eta = (\sigma_{UV}/\sigma^L_{UV}) = 1.0$) (upper), and ($\xi = (\varepsilon_{UV}/\varepsilon^B_{UV}) \approx 0.89$, $\eta = (\sigma_{UV}/\sigma^L_{UV}) \approx 0.87$) (lower).

the asymmetry of the $^3BP - CO_2$ interactions, and therefore, to change the sign of the pressure dependence in the reaction $^3BP + {}^3O_2 + CO_2 \Leftrightarrow TS$ from $(\partial \ln k^{TST}/\partial P)_{T,x} > 0$ to $(\partial \ln k^{TST}/\partial P)_{T,x} < 0$ (Figs. 17a, b). Likewise, deviations of $\xi = (\varepsilon_{UV}/\varepsilon_{UV}^{B}) \approx 0.89$ and $\eta = (\sigma_{UV}/\sigma_{UV}^{L}) \approx 0.87$ for the $TS - CO_2$ in the $^3BP + 1{,}4\_C_6 + CO_2 \Leftrightarrow TS$, will reverse the sign of $(\partial \ln k^{TST}/\partial P)_{T,x}$ from positive to negative (Figs. 18a, b).

## 3.4. Ion Solvation

Here we present a few results for *CsBr* in an infinitely dilute aqueous-type solution, along three supercritical isotherms (643 K, 673 K, and 703 K), and within the density range of $0.0136 \leqslant \rho(\text{g/cm}^3) \leqslant 0.81$. The system is defined as charged hard sphere ions immersed in a model aqueous-like solvent, described as a hard sphere with an embedded point polarizability and permanent electrostatic multipole moments (including quadrupole and octupoles). The effect of the solvent polarizability is taken into account by using the self-consistent mean field approach (SCMF) as described elsewhere.[54, 55] In contrast to the earlier calculations of Kusalik and Patey,[54, 55] here the ions bear only a 66% of the full charge. The reduced charges were necessary to avoid the collapse of solvent molecules on bare ions, and thus, ensure the convergence of the integral equation calculations over the entire solvent density range considered. (The RHNC integral equation theory appears to predict a shifting upwards of the phase coexistence envelope due to the perturbing effects of bare unscreened ionic charges. These effects can be reduced by increasing the size of the ions or by decreasing the ionic charge).

Here we target the $T - \rho$ dependence of $D_{UV}^{\infty} = (\kappa^{IG}/\kappa)\, \bar{v}_U^{\infty}$ from a molecular viewpoint, where $\kappa$ and $\bar{v}_U^{\infty}$ are the isothermal compressibility of the solvent and the partial molar volume of the ionic solute (salt) at infinite dilution, and the superscript *IG* denotes the ideal gas behavior. This quantity is currently the focus of much attention because of its intriguingly weak temperature-dependence in the range of $550 < T(\text{K}) < 725$,[56, 57] which makes it very attractive for regression purposes. For example, in Fig. 19 we present the RHNC predicted solvent density-dependence of $D_{UV}^{\infty}$ along the three supercritical isotherms for infinitely dilute *CsBr* aqueous-like solutions. Note that, according to the predicted relation between $\kappa$ and $\rho$ along the isotherm $T = 643$ K, the critical point of this water-like solvent is $T_c \approx 643$ K and $\rho_c \approx 0.20$ g/cm$^3$, i.e., the three isotherms considered here are supercritical. We also compare these results with the corresponding experimental data of Sedlbauer *et al.*,[57] which were determined from measurements of solute partial molar volumes at infinite dilution within the temperature and density ranges $604 < T(\text{K}) < 717$ and $0.26 < \rho(\text{g/cm}^3) <$

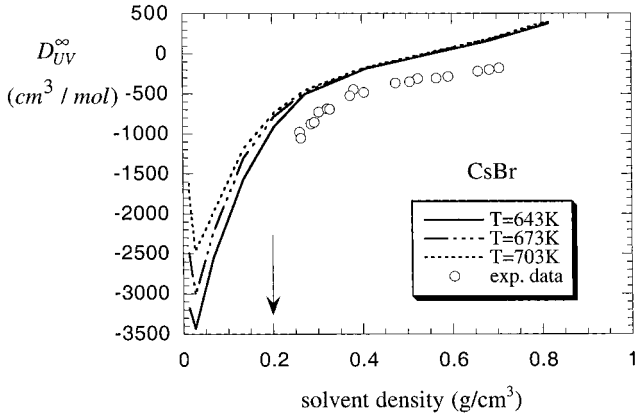


Fig. 19. Behavior of $D^{\infty}_{UV} = (\kappa^{IG}/\kappa)\,\bar{v}^{\infty}_{U}$ for an infinitely dilute *CsBr* aqueous solution as a function of the solvent density along three supercritical isotherms in comparison with experimental data. Arrow indicates the estimated critical density of the model solvent.

0.60, respectively. The outstanding feature of the predicted values of $D^{\infty}_{UV}$ is their lack of temperature dependence for supercritical densities, an appealing behavior that prompts some relevant questions regarding the underlying microscopic mechanism. Incidentally, this is the same behavior observed previously for several types of high-temperature electrolyte and non-electrolyte aqueous solutions.[56–58]

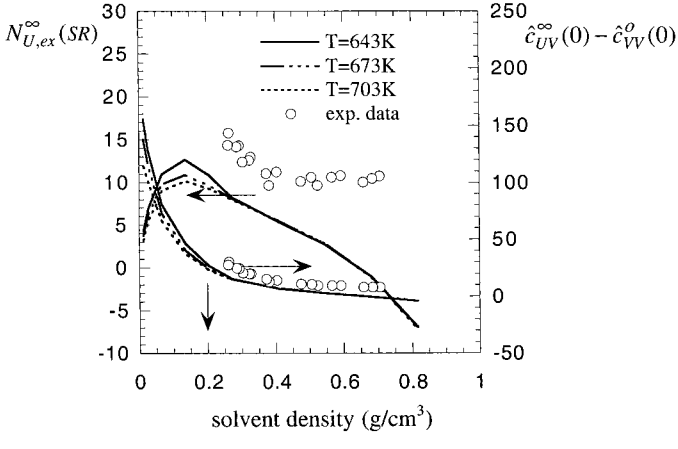


Fig. 20. Behavior of $N^{\infty}_{U,ex}(SR)$ and $(C^{\infty}_{UV} - C^{0}_{VV})/\rho$ for an infinitely dilute *CsBr* aqueous solution as a function of the solvent density along three supercritical isotherms in comparison with experimental data. Vertical arrow indicates the estimated critical density of the model solvent.

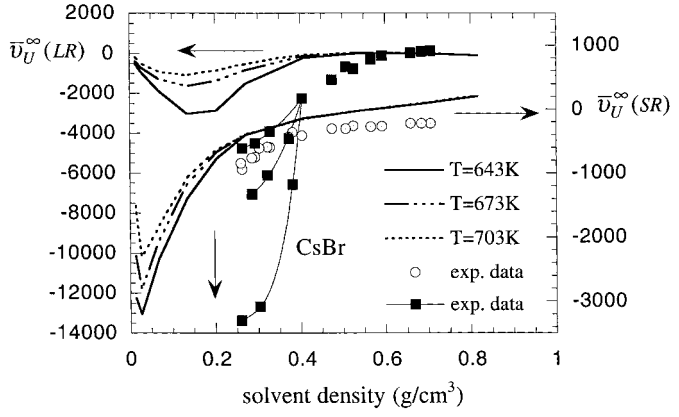


Fig. 21. Behavior of $\bar{v}_U^{\infty}(SR)$ and $\bar{v}_U^{\infty}(LR) \equiv \bar{v}_U^{\infty} - \bar{v}_U^{\infty}(SR)$ for an infinitely dilute *CsBr* aqueous solution as a function of the solvent density along three supercritical isotherms in comparison with experimental data. Vertical arrow indicates the estimated critical density of the model solvent. The three lines joining the experimental data correspond approximately to the isotherms of 669 K, 686 K, and 709 K from bottom to top, respectively.

For example, the weak temperature-dependence exhibited by $D_{UV}^{\infty}$ [12, 13] can be interpreted in terms of $N_{U,ex}^{\infty}(SR)$ (see Fig. 20), a quantity that also displays a clearly negligible temperature-dependence for supercritical densities. Yet another way to interpret the previously mentioned weak temperature dependence is through the analysis of the two contributions to the solute partial molar volume $\bar{v}_U^{\infty}$, i.e., the solvation $\bar{v}_U^{\infty}(SR)$, and the compressibility-driven $\bar{v}_U^{\infty}(LR)$ contributions, respectively. From Fig. 21 it is clear that the solvation portion $\bar{v}_U^{\infty}(SR)$ (as opposed to the compressibility-driven portion $\bar{v}_U^{\infty}(LR)$) exhibits the negligible temperature dependence found in the associated quantities (Figs. 19 and 20), and highlights once again the appeal of well-defined solvation quantities as the target for regression purposes.

## 4. DISCUSSION AND FINAL REMARKS

We have briefly described the solvation process in high-temperature solutions based on thermodynamic and statistical mechanical views, and according to the discrimination between the true solvation phenomena and the largely unrelated accompanying compressibility-driven phenomena. The solvation-related properties (here designated as "*SR*") bear unambiguous microscopic meaning, and can be interpreted macroscopically in

terms of the isothermal compressibility of the pure solvent $\kappa$ and the infinite-dilution partial molar properties.[13] For example,

$$\bar{v}_U^{\infty}(SR) = (\kappa^{IG}/\kappa)(\bar{v}_U^{\infty} - v v_V^o) + v v_V^o \tag{35}$$

and, consequently,

$$N_{U,ex}^{\infty}(SR) = (\kappa^{IG}/\kappa)(v - (\bar{v}_U^{\infty}/v_V^o)) \tag{36}$$

This excess number $N_{U,ex}^{\infty}(SR)$ (and its individual ion counterparts) should not be confused with the traditional idea of coordination number (the geometric arrangement of solvent molecules around a central species), and consequently, it cannot be associated with the conventional solvation numbers obtained through *NMR*, *EXAFS*, neutron or *x*-ray diffraction measurements.[59, 60] In fact, $N_{U,ex}^{\infty}(SR)$ accounts for the solvent molecules *directly correlated* with the central species in excess over that in which the central molecule is another solvent molecule (the ideal solution in the Lewis–Randall sense). Note also that, while $N_{U,ex}^{\infty}(SR)$ encompasses unambiguous connections with all solvation properties, the more familiar concept of solvation numbers does not.[13]

Because this solvation approach hinges upon the rigorous Kirkwood–Buff's fluctuation formalism of mixtures, and it is applied to precisely-defined model mixtures, we are able to make unambiguous connections between the species molecular asymmetries, the solution microstructure, and the solvation-relevant macroscopic properties. Even though the solvation formalism was derived for molecules of arbitrary symmetry, we applied it first to simple model mixtures for which integral equation calculations provide accurate predictions. These calculations allow us not only to generate the microstructural details of the systems, but also to calculate the required macroscopic properties relevant to high-temperature solvation phenomena. In doing so, we maintain an internal consistency between the microstructure and the corresponding (macroscopic) thermophysical properties.

Subsequently, and considering that the target of the molecular-based studies is the development of successful engineering correlations, the solvation formalism becomes a powerful tool for interpreting of experimental data and for choosing the best combination of properties for regression purposes.

## ACKNOWLEDGMENTS

The authors are pleased to dedicate this paper to their colleague, friend and mentor George Stell on the occasion of his 65th birthday. In this

paper, we have shown how the judicious use of integral equation methods continues to be vital tool in understanding supercritical fluid mixtures. Many of the kinds of systems and methods favored by George and studied by him over the years are represented in this paper. PTC and YuVK are particularly pleased to acknowledge the personal satisfaction each has derived from working with George directly, PTC as a postdoctoral research associate during the period 1981–1983, and YuVK over more than a decade. Both of us have been privileged to have interacted with George and learned much about treading the fine line between taking ourselves and our science too seriously and not taking it seriously enough. We thank you, George, for your friendship, guidance, and concern for our personal and professional lives.

This research was sponsored by the Division of Chemical Sciences, Office of Basic Energy Sciences, U.S. Department of Energy at Oak Ridge National Laboratory, managed by Lockheed Martin Energy Research Corporation for the U.S. Department of Energy under contract DE-AC05-96OR22464. PTC was supported by the Division of Chemical Sciences, Office of Basic Energy Sciences, U.S. Department of Energy. PGK acknowledges the financial support of the Natural Sciences and Engineering Research Council of Canada.

## REFERENCES

1. T. J. Bruno and J. F. Ely, *Supercritical Fluid Technology* (CRC Press, Boca Raton, 1991).
2. E. Kiran and J. M. H. Levelt Sengers, *Supercritical Fluids. Fundamentals for Applications* (Kluwer Academic Publishers, Dordrecht, 1994).
3. Anonymous, in *Food Engineering International* (1981), pp. 45–46.
4. P. Hubert and O. G. Vizthum, *Angew. Chem. Int. Ed. Engl.* **17**:710–715 (1978).
5. M. Modell, in *Standard Handbook of Hazardous Waste Treatment and Disposal*, H. M. Freeman, ed. (McGraw–Hill, New York, 1989).
6. P. E. Savage, S. Golapan, T. I. Mizan, C. J. Martino, and E. E. Brock, *AICHE J.* **41**:1723–1778 (1995).
7. A. A. Chialvo and P. T. Cummings, *AICHE J.* **40**:1558–1573 (1994).
8. J. M. H. Levelt Sengers, *J. Supercritical Fluids* **4**:215–222 (1991).
9. D. B. McGuigan and P. A. Monson, *Fluid Phase Equilibria* **57**:227–247 (1990).
10. L. L. Lee, P. G. Debenedetti, and H. D. Cochran, in *Supercritical Fluid Technology: Reviews in Modern Theory and Applications*, T. J. Bruno and J. F. Ely, eds. (CRC Press, Boca Raton, 1991), pp. 193–226.
11. A. A. Chialvo and P. T. Cummings, in *Advances in Chemical Physics*, Vol. 109, S. A. Rice, ed. (Wiley & Sons, New York, 1999), pp. 115–205.
12. A. A. Chialvo and P. T. Cummings, *Molec. Phys.* **84**:41–48 (1995).
13. A. A. Chialvo, P. T. Cummings, J. M. Simonson, and R. E. Mesmer, *J. Chem. Phys.* **110**:1075–1086 (1999).
14. A. A. Chialvo, *J. Chem. Phys.* **92**:673–679 (1990).
15. A. A. Chialvo, *Fluid Phase Equilibria* **83**:23–32 (1993).

16. A. A. Chialvo, P. T. Cummings, J. M. Simonson, and R. E. Mesmer, *J. Molecular Liquids*, in press (2000).
17. P. G. Kusalik and G. N. Patey, *J. Chem. Phys.* **86**:5110–5116 (1987).
18. J. P. O'Connell, in *Fluctuation Theory of Mixtures*, Vol. 2, E. Matteoli and G. A. Mansoori, eds. (Taylor and Francis, New York, 1990), pp. 45–67.
19. M. Modell and R. C. Reid, *Thermodynamics and its Applications* (Prentice–Hall, Englewood Cliffs, New Jersey, 1983).
20. M. E. Paulaitis, V. J. Krukonis, R. T. Kurnik, and R. C. Reid, *Rev. Chem. Eng.* **1**:179–250 (1983).
21. M. L. Japas and J. M. H. Levelt Sengers, *AICHE J.* **35**:705–713 (1989).
22. A. H. Harvey and J. M. H. Levelt Sengers, *AICHE J.* **36**:539–546 (1990).
23. A. H. Harvey, R. Crovetto, and J. M. H. Levelt Sengers, *AICHE J.* **36**:1901–1904 (1990).
24. W. Wilhelm, in *Molecular Liquids: New Perspectives in Physics and Chemistry*, J. J. C. Teixeira-Dias, ed. (Kluwer Academic Publishers, 1992), pp. 175–206.
25. A. A. Chialvo, Y. V. Kalyuzhnyi, and P. T. Cummings, *AICHE J.* **42**:571–584 (1996).
26. J. F. Brennecke, in *Supercritical Engineering Science. Fundamentals Studies and Applications*, Vol. 514, E. Kiran and J. F. Brennecke, eds. (American Chemical Society, Washington, DC, 1993), pp. 201–219.
27. C. E. Bunker and Y.-P. Sun, *J. Am. Chem. Soc.* **117**:10865–10870 (1995).
28. J. E. Chateauneuf, C. B. Roberts, and J. F. Brennecke, in *Supercritical Fluid Technology. Theoretical and Applied Approaches in Analytical Chemistry*, Vol. 488, F. V. Bright and M. E. P. McNally, eds. (American Chemical Society, Washington, 1992), pp. 106–120.
29. J. T. Hynes, in *Theory of Chemical Reaction Dynamics*, Vol. IV, M. Baer, ed. (CRC Press, Boca Raton, 1985), pp. 171–234.
30. A. A. Chialvo, P. T. Cummings, and Y. V. Kalyuzhnyi, *AICHE J.* **44**:667–680 (1998).
31. J. M. H. Levelt Sengers, in *Supercritical Fluid Technology*, T. J. Bruno and J. F. Ely, eds. (CRC Press, Boca Raton, 1991a), pp. 1–56.
32. A. A. Chialvo, P. G. Kusalik, P. T. Cummings, and J. M. Simonson, *J. Chemical Physics*, submitted for publication (2000).
33. P. G. Kusalik and G. N. Patey, *J. Chem. Phys.* **89**:5845–5851 (1988).
34. P. H. Fries and G. N. Patey, *J. Chem. Phys.* **82**:429–440 (1985).
35. A. A. Chialvo and P. G. Debenedetti, *Industrial & Engineering Chemistry Research* **31**:1391–1397 (1992).
36. B. L. Knutson, D. L. Tomasko, C. A. Eckert, P. G. Debenedetti, and A. A. Chialvo, in *Recent Advances in Supercritical Fluid Technology. Theoretical and Applied Approaches to Analytical Chemistry*, Vol. 488, F. Bright and M. E. P. McNally, eds. (American Chemical Society, Washington, DC, 1992), pp. 61–72.
37. J. A. O'Brien, T. W. Randolph, C. Carlier, and G. Shankar, *AICHE J.* **39**:1061–1071 (1993).
38. P. G. Debenedetti and R. S. Mohamed, *J. Chem. Phys.* **90**:4528–4536 (1989).
39. D. Henderson, E. Waisman, J. L. Lebowitz, and L. Blum, *Molec. Phys.* **35**:241–255 (1978).
40. L. S. Ornstein and F. Zernike, *Proc. Akad. Sci. (Amsterdam)* **17**:793–806 (1914).
41. E. Arrieta, C. Jedrzejek, and K. M. Marsh, *J. Chem. Phys.* **95**:6838–6848 (1991).
42. Y. V. Kalyuzhnyi and P. T. Cummings, *Molec. Phys.* **87**:1459–1462 (1996).
43. J. S. Høye and G. Stell, *J. Chem. Phys.* **67**:439 (1977).
44. A. A. Chialvo, Y. Kalyuzhnyi, and P. T. Cummings, in *Innovations in Supercritical Fluids: Science and Technology*, Vol. 608, K. W. H. a. N. R. and Foster, eds. (American Chemical Society, Washington, DC, 1995), pp. 34–46.
45. C. Ebner, W. F. Saam, and D. Stroud, *Phys. Rev. A* **14**:2264–2272 (1976).
46. R. J. Baxter, *J. Chem. Phys.* **52**:4559 (1970).

47. J. S. Høye, E. Waisman, and G. Stell, *Molec. Phys.* **32**:209 (1976).
48. J. S. Høye and L. Blum, *J. Stat. Phys.* **16**:399 (1977).
49. Y. V. Kalyuzhnyi and M. F. Holovko, *Molec. Phys.* **80**:1165–1176 (1993).
50. K. P. Shukla, A. A. Chialvo, and J. M. Haile, *Industrial & Engineering Chemistry Research* **27**:664–671 (1988).
51. A. A. Chialvo and P. G. Debenedetti, *Molec. Simulation* **7**:265–283 (1991).
52. C. B. Roberts, J. Zhang, J. E. Chateauneuf, and J. F. Brennecke, *J. Am. Chem. Soc.* **117**:6553–6560 (1995).
53. A. A. Chialvo, *Molec. Phys.* **73**:127–140 (1991).
54. P. G. Kusalik and G. N. Patey, *J. Chem. Phys.* **88**:7715–7738 (1988).
55. P. G. Kusalik and G. N. Patey, *J. Chem. Phys.* **89**:7478–7484 (1988).
56. J. P. O'Connell, A. V. Sharygin, and R. H. Wood, *Industrial & Engineering Chemistry Research* **35**:2808–2812 (1996).
57. J. Sedlbauer, E. M. Yezdimer, and R. H. Wood, *J. Chem. Thermodyn.* **30**:3–12 (1998).
58. M. S. Gruszkiewicz and R. H. Wood, *J. Phys. Chem. B* **101**:6549–6559 (1997).
59. M. Magini, G. Licheri, G. Paschina, G. Piccaluga, and G. Pinna, *X-Ray Diffraction of Ions in Aqueous Solutions: Hydration and Complex Formation* (CRC Press, Inc., Boca Raton, 1988).
60. B. E. Conway, *Ionic Hydration in Chemistry and Biophysics* (Elsevier, Amsterdam, 1981).